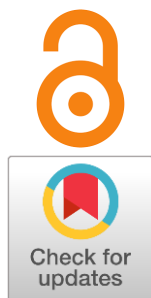ARTICLE

Electrochemical Materials and Technologies

Co-doping effect on the microstructural and electrical properties of barium stannate materials

George Starostin [a] [*], Mariam Akopian [a], Inna Starostina [a], Dmitry Medvedev [a] [*]

Proton-conducting perovskite oxides are of considerable interest to researchers as promising electrolytes for low- and intermediate solid oxide electrochemical cells. Therefore, designing new potential proton-conducting phases and improving the functional properties of known materials are of great importance from both fundamental and applied viewpoints. In the present work, $BaSnO_3$ was selected as a reference proton-conducting system and then a co-doping strategy was employed to analyze 'composition – structure – microstructure – transport properties' relationships. To perform such an analysis, the properties of previously studied $BaSn_{0.7}M_{0.3}O_{3-\delta}$ (M = In, Sc, Y) compounds were compared here to their co-doped derivatives, $BaSn_{0.7}In_{0.15}Sc_{0.15}O_{3-\delta}$, $BaSn_{0.7}Y_{0.15}Sc_{0.15}O_{3-\delta}$, and $BaSn_{0.7}In_{0.15}Y_{0.15}O_{3-\delta}$. It is found that the type of dopant affects the materials sinterability, when more coarse-crystalline ceramics are formed with increasing the average ionic radii at the Sn-position. The introduction of Y^{3+}-cations reduces both ionic and hole conductivities compared to single-doped with In^{3+} or Sc^{3+} barium stannate materials. However, simultaneous doping with In^{3+}/Sc^{3+} cations minimizes the contribution of hole conductivity compared to that of Sc-doped barium stannate with the same acceptor dopant concentration.

1. Introduction

Hydrogen energy is a promising direction in the development of alternative energy sources that meets the requirements of environmental friendliness and renewability [1, 2]. One of the key devices for hydrogen energy solutions are solid oxide fuel cells (SOFCs) and solid oxide electrolysis cells (SOECs). These are electrochemical devices for direct conversion of chemical energy of fuel into electricity and vice versa, being attractive for a wide range of applications, including stationary and mobile power supplies [3, 4]. In addition, SOECs are utilized to produce hydrogen by electrochemical splitting of water into oxygen and hydrogen when an electrical current is applied. The improvement of efficiency, operation time, and reliability

of these devices can be achieved by varying the properties of their constitute functional materials, including electrolyte, cathode, anode, interconnector, and glass sealant [5, 6]. In particular, the SOFC/SOEC operating temperatures can be significantly reduced by utilizing proton-conducting electrolyte materials instead of conventional oxygen-ionic electrolytes. Proton transport has been found for many complex oxides, including perovskites, fergusonites/scheelites, braunmillerites, fluorites, apatites, mayenites, etc. [7, 8].

$BaSnO_3$-based materials are of interest due to their perovskite structure and proton conductivity [9]. Such stannates belong to a family of perovskite-related proton-conducting oxides, which is extensively studied. This family includes materials based on alkaline-earth cerates ($SrCeO_3$, $BaCeO_3$), zirconates ($CaZrO_3$, $SrZrO_3$, $BaZrO_3$), hafnates ($CaHfO_3$, $SrHfO_3$, $BaHfO_3$), and some others [10, 11]. Literature analysis reveals that the co-doping strategy is widely employed in the mentioned systems, until the design of high- or medium-entropy oxide systems [12, 13]. This is due to the fact that single-doping is often

a: Institute of High Temperature Electrochemistry, Yekaterinburg 620066, Russia

* Corresponding author: gorgge23@mail.ru (G.N. Starostin), dmitrymedv@mail.ru (D.A. Medvedev)

insufficient to achieve an optimum between different functional properties. Conversely, research on stannates is primarily limited to single-doped materials, such as In-doped [14–16], Y-doped [9, 17, 18], and Sc-doped [19, 20] compounds. In these examples, the functional properties of the stannate materials are closely related to changes in composition, specifically the content of acceptor dopants. This, in turn, affects the defect and structural properties of the materials. However, it is difficult to separate these effects from each other. Changing the type of dopants while maintaining their overall concentration is a suitable chemical modification approach that minimizes the influence of defects. Only two studies have investigated co-doping of the Sn-site in barium stannate [21, 22]. In one of these studies, Zn^{2+} was used as a dopant along with Y^{3+} [21], which has a different oxidation state than both Y^{3+} and Sn^{4+} cations. As a result, the defect structure is proposed to have been altered. The second work [22] discusses the highly doped compositions, $BaSn_{0.5}Y_{0.5-x}In_xO_{3-\delta}$, which were obtained upon the partial substitution of Y^{3+} with In^{3+} cations. However, a high concentration of acceptor dopants may destabilize the perovskite structure, leading to the formation of a brownmillerite-based phase with ordered oxygen vacancies [23, 24]. Therefore, this work presents a comparative overview of the co-doping and single-doping effect on the functional properties of barium stannate materials, whose crystal structure remains stable under a medium concentration of introduced dopant(s).

2. Experimental

The co-doped $BaSn_{0.7}Y_{0.15}Sc_{0.15}O_{3-\delta}$ (denoted as BSY-Sc), $BaSn_{0.7}In_{0.15}Sc_{0.15}O_{3-\delta}$ (BSIn-Sc), $BaSn_{0.7}In_{0.15}Y_{0.15}O_{3-\delta}$ (BSIn-Y), and $BaSn_{0.7}In_{0.3}O_{3-\delta}$ (BSIn) powders were produced via the solid-state synthesis route using $BaCO_3$ (99.98 % Sigma-Aldrich, USA), SnO_2 (99.9 % Sigma-Aldrich, USA), Y_2O_3 (99.9 % Sigma-Aldrich, USA), Sc_2O_3 (99.9 % Sigma-Aldrich, USA), In_2O_3 (99.99 % Alfa Aesar, USA) as starting reagents. The components were dried, weighed in stoichiometric ratios and then thoroughly grinded employing a planetary ball mill (Pulverisette 7 premium line, FRITSCH, Germany) with YSZ milling balls in an acetone medium for 2 h. The mixtures were dried and then calcined at 1200 °C for 5 h in air to provide full decomposition of $BaCO_3$ and preliminary synthesis. Afterwards, the calcined powders were mixed with 0.5 wt. % CuO as a sintering additive and cold uniaxial pressed at 140 MPa into cylindrical samples. Finally, the latter were sintered at 1450 °C (5 h) for co-doped barium stannates, at 1350 °C (5 h) for BSIn. These sintering parameters were selected by preliminary

experiments to satisfy the following conditions simultaneously: (i) achieving a pure phase with no impurities as initial oxides or reaction products; (ii) producing gas-tight ceramics; (iii) obtaining all three co-doped pairs under close conditions to provide the comparison of those properties tailored by the dopant nature.

The phase state of the samples was studied by X-ray diffraction (XRD) analysis using a Rigaku MiniFlex 600 diffractometer (Rigaku Co. Ltd., Japan) in CuKα radiation ($\lambda = 1.54056$ Å) in Bragg-Brentano geometry from 10 ° to 90 ° 2θ range at a scan rate of 0.3 ° · min^{-1}. The lattice parameters were refined by Rietveld refinement analysis using a FullProf software. The surface morphology of both the as-prepared and polished ceramic samples was investigated in the back-scattered electron (BSE) mode using a scanning electron microscope (TESCAN MIRA III, TESCAN s.r.o., Czech Republic) equipped with an emission Schottky cathode (a 15 keV accelerating voltage at a current of 300 pA). An Image J software tool was utilized to estimate the average grain size of the ceramic samples from their micrographs.

Electrical properties of the ceramic samples were investigated using a DC four-probe method of electrical conductivity measurement. In detail, each bar-shaped sample was placed into a specially designed YSZ-cell equipped with platinum electrodes acting as electrochemical oxygen pump and sensor. A Pt-Pt/Rh thermocouple was placed alongside the sample for maintaining the oven temperature with an accuracy of ± 1 °C. A Zirconia-318 automatic microprocessor controller was used to regulate the temperature and oxygen partial pressure (pO_2) inside the measurement cell. The measurements were performed at $pO_2 = 0.21$ and $pO_2 = 10^{-8}$ atm under cooling in the temperature range of 500–900 °C with a step of 25 °C and exposure for 1 h/step to equilibrate the sample with the gas atmosphere.

3. Results and discussion

3.1. Crystal structure and surface morphology

Barium stannates co-doped with Y/Sc, In/Sc, and In/Y cations in equal ratios were obtained in the form of single-phase ceramic samples as confirmed by the XRD analysis (Figure 1). An ICDD PDF-2 card for the nearest $BaSn_{0.75}Y_{0.25}O_{3-\delta}$ phase composition was used to fit the obtained XRD spectra, while the XRD data were analyzed by the Rietveld refinement method (Table 1). According to these results, all the samples crystallize into a cubic perovskite-type structure (space group $Pm\bar{3}m$). Co-doping with acceptor dopants leads to a lattice expansion

compared to undoped barium stannate, that is in agreement with differences between the ionic radii of tin $r(Sn^{4+}) = 0.69$ Å in VI coordination state and the dopants of $r(Sc^{3+}) = 0.745$ Å, $r(In^{3+}) = 0.8$ Å, and $r(Y^{3+}) = 0.9$ Å. The Goldschmidt tolerance factor calculated according to Eqn (1) for all investigated compositions is close to unity similarly to single-doped barium stannates, which confirms the formation of highly symmetric structures.

$$t = \frac{r_A + r_O}{\sqrt{2}(r_B + r_O)}, \qquad (1)$$

where, r_A is the ionic radius of the A-site cation, r_O is the ionic radius of the oxygen, r_B is the ionic radius of the B-site cation, calculated for co-doped barium stannates as follows:

$$r_B = 0.7r_{Sn} + 0.15r_{In/Y/Sc} + 0.15r_{In/Y/Sc}, \qquad (2)$$

here, r_{Sn} is is the ionic radius of the tin, while $r_{In/Y/Sc}$ is the ionic radius of the corresponding cations in BSIn-Sc, BSIn-Y, BSY-Sc pairs.
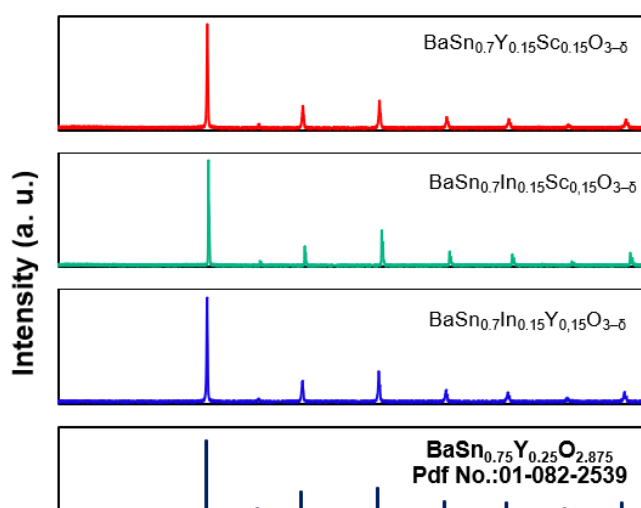

Figure 1 X-ray diffraction patterns of the co-doped barium stannate ceramic materials and an example of ICDD PDF-2 card for the more suitable barium stannate phase with a close concentration of acceptor dopant.

Table 1 – Lattice parameters for acceptor-doped barium stannate samples and corresponding values of the Goldschmidt tolerance factor (t).

Composition	a (Å) ± 0.001 Å	V (Å^3) ± 0.1 Å	t	Ref.
$BaSn_{0.7}Y_{0.15}Sc_{0.15}O_{3-\delta}$	4.163	72.15	1.00	This work
$BaSn_{0.7}In_{0.15}Sc_{0.15}O_{3-\delta}$	4.141	71.01	1.01	
$BaSn_{0.7}In_{0.15}Y_{0.15}O_{3-\delta}$	4.174	72.72	1.00	
$BaSn_{0.7}Sc_{0.3}O_{3-\delta}$	4.139	70.91	1.01	[19]
$BaSn_{0.7}Y_{0.3}O_{3-\delta}$	4.199	74.04	0.99	[25]
$BaSnO_3$	4.117	69.78	1.02	[25]

Figure 2 shows SEM-images of the as-prepared co-doped (top line) ceramic materials versus the single-doped (bottom line) $BaSn_{0.7}(Sc/Y/In)_{0.3}O_{3-\delta}$ samples investigated earlier by our group [19,25]. The surface of the yttrium-containing BSY-Sc, BSIn-Y samples is characterized by some visible defects and pores, whereas the formation of spherical-like grains is found for the BSIn-Sc ceramic materials. Similar trends are observed for the single-doped ceramics.

In general, the microstructural parameters are closely related to the transport properties due to the specific features of proton transport through the ceramic grain boundaries. According to the space charge layer model, a double electric layer is formed near the grain boundaries acting as an energy barrier for proton transport [26]. Therefore, decreasing the area of grain boundaries is favorable for increasing the ionic conductivity [27]. In a number of studies, bulk and grain boundary transport of proton conductors have been analyzed in a combination with the microstructural parameters of the as-prepared ceramics related to their surface. However, this approach might be incorrect since grains often appear to have a different shape within the ceramic volume, which can be clearly seen from the comparison of Figures 2 and 3. This difference in the microstructural properties of the surface and volume of the ceramic materials might be explained by different densification kinetics of the internal grains compared to the surface grains.

The approach of using sintering additives is widely used to produce complex oxides being refractory in nature, including barium stannates and related systems based on barium zirconate [24]. The densification of such ceramic materials occurs at temperatures above 1600 °C, being unfavorable due to the evaporation (or volatility) of BaO during the fabrication of bulk samples, as well as the interfacial interaction when producing the multilayer structures [9, 13]. In this work, we used CuO as a sintering agent. This agent has a low melting point [28, 29] and tends to accumulate at the surface or grain boundaries, affecting sinterability and grain growth in different areas of the ceramic material.

According to these SEM-images (Figure 3), all the obtained co-doped ceramic materials exhibit a dense packing of grains with no visible pores and other volume defects, confirming high relative density of the samples (above 97 %). A wide palette of gray shades of the grains is related to intergranular contrast due to their different grain orientation; this is not related to different chemical compositions of these grains. Although the barium stannates were doped in equal concentrations of acceptor dopants, the resulting grain size for the ceramic samples is notably different. Its size increases in the series of BSIn-Sc

(1.8 μm) → BSY-Sc (2.2 μm) → BSIn-Y (2.8 μm). This interesting result indicates that the densification of the studied materials is regulated by not only the CuO sintering additive, but also the nature of the introduced dopants. The literature analysis suggests that an increase in the ionic radius of M^{3+} in $BaCe_{1-x-y}Zr_xM_yO_{3-\delta}$ perovskites promotes more active sintering of samples, resulting in an increase in relative density, shrinkage, and grain size. This trend is observed for cerates ($x = 0$ [30]), zirconates ($x = 1 - y$ [31]), and mixed systems ($0 < x < 1 - y$ [32]) regardless of their preparation techniques. Based on these results, it is clear that a greater densification takes place for larger perovskite crystals. In other words, doping with high ionic radii elements is a

viable method for enhancing the sinterability of Ba-based stannates, cerates, and zirconates. However, it is important to note that at very high ionic radii, dopants introduced to the B-position of such ABO_3 perovskites can replace Ba-ions at the A-sites during sintering. Therefore, it is crucial to use rational dopant elements under the preparation of desired phases.

Figure 4 shows the energy-dispersive X-ray spectroscopy data for the co-doped stannates. The presented spectra contain only those elements that exist in the synthesized phases. At the same time, the cationic compositions are found to be close to nominal ones for all cases, taking a detection error of ± 0.01 mol % into account.
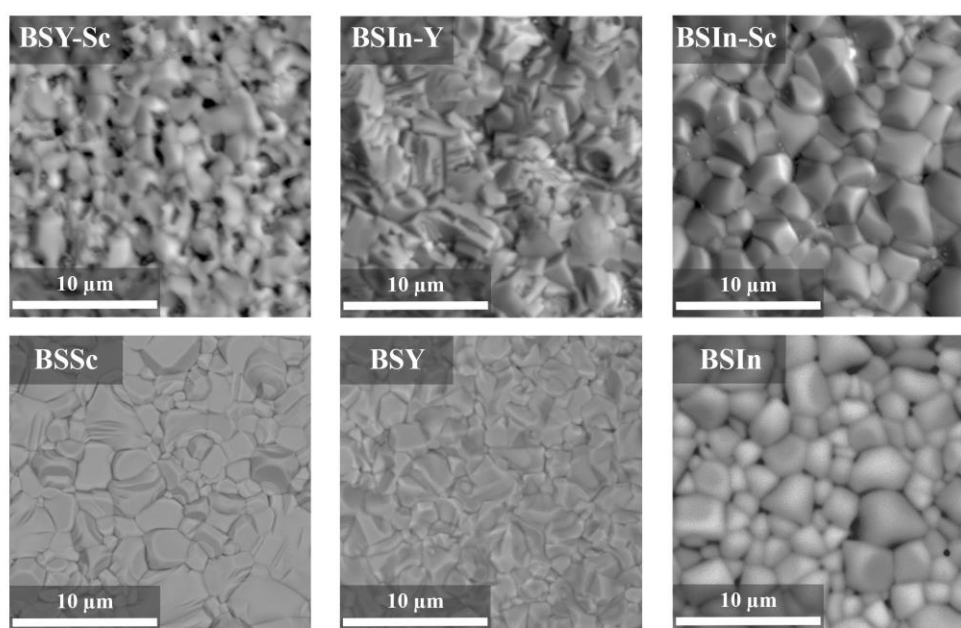

Figure 2 Scanning electron microscopy (SEM) data for the co-doped ceramic samples: $BaSn_{0.7}Y_{0.15}Sc_{0.15}O_{3-\delta}$ (BSY-Sc), $BaSn_{0.7}In_{0.15}Y_{0.15}O_{3-\delta}$ (BSIn-Y), $BaSn_{0.7}In_{0.15}Sc_{0.15}O_{3-\delta}$ (BSIn-Sc) (top line) and single-doped (bottom line) $BaSn_{0.7}(Sc/Y/In)_{0.3}O_{3-\delta}$ ceramic samples [19, 25].

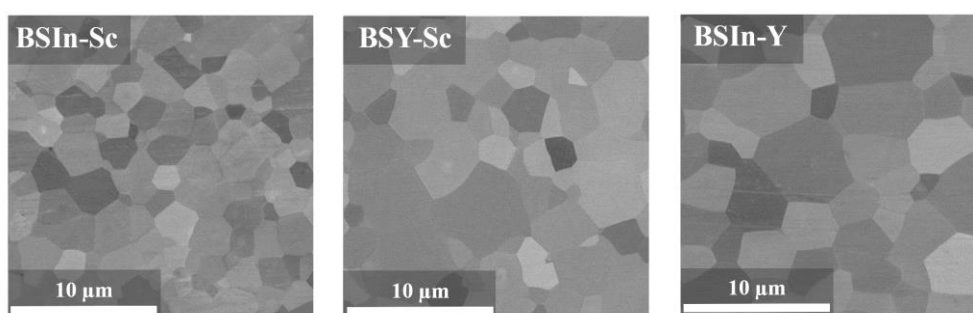**Figure 3** SEM-images for the polished $BaSn_{0.7}In_{0.15}Sc_{0.15}O_{3-\delta}$ (BSIn-Sc), $BaSn_{0.7}Y_{0.15}Sc_{0.15}O_{3-\delta}$ (BSY-Sc) and $BaSn_{0.7}In_{0.15}Y_{0.15}O_{3-\delta}$ (BSIn-Y) ceramic samples.
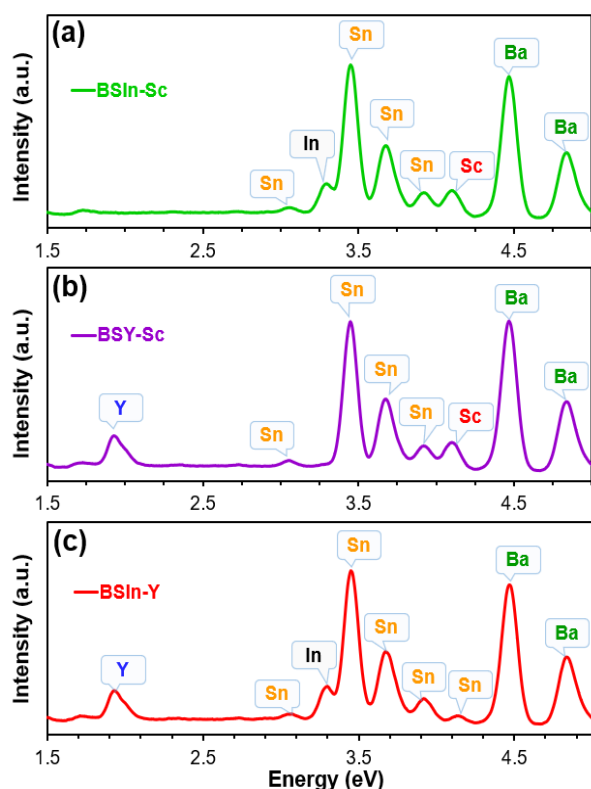
Figure 4 The energy-dispersive X-ray spectroscopy data for the co-doped barium stannates: (a) $BaSn_{0.7}In_{0.15}Sc_{0.15}O_{3-\delta}$ (BSIn-Sc); (b) $BaSn_{0.7}Y_{0.15}Sc_{0.15}O_{3-\delta}$ (BSY-Sc) and (c) $BaSn_{0.7}In_{0.15}Y_{0.15}O_{3-\delta}$ (BSIn-Y).

3.2. Transport properties

Barium stannate, similar to other proton-conducting materials, including those based on $BaCeO_3$, $BaZrO_3$, $LaYbO_3$, etc., is a mixed ionic-electronic conductor [33, 34]. Oxygen ions, protons, electrons or electron holes may act as charge carriers depending on external conditions such as temperature, humidity, and oxygen partial pressure (pO_2). The mentioned complex oxides demonstrate hole conductivity in the region of high pO_2 values. The region of intermediate and low pO_2 values represents the as-called "ionic plateau", where the conductivity remain unchanged. The width of the ionic plateau can be varied depending on the composition, reaching pO_2 values up to 10^{-5} atm for acceptor-doped barium stannates [19, 25]. The temperature dependence of conductivity for the co-doped ceramic samples was measured under two conditions: (i) in wet air atmosphere ($pO_2 = 0.21$ atm, $pH_2O = 0.02$ atm) to evaluate the hole contribution to the total conductivity; (ii) under low oxygen partial pressure conditions at $pO_2 = 10^{-8}$ atm to evaluate the ionic transport.

Figure 5 presents the temperature dependences of electrical conductivity for the co-doped samples compared to single-doped $BaSn_{0.7}(Sc/Y/In)_{0.3}O_{3-\delta}$ barium stannates. An increase in conductivity is observed for all the samples with temperature growth under both low and high pO_2 values. The conductivity values attributed to the hole component increase linearly for the co-doped samples at $pO_2 = 0.21$ atm. The electrical conductivity dependences in the electrolytic region at $pO_2 = 10^{-8}$ atm show a bend at the temperature of ~ 750 °C. The observed bend for co-doped samples may be associated with the change of the dominant type of charge carriers from protons to oxygen-ions at such temperatures due to dehydration process [35].
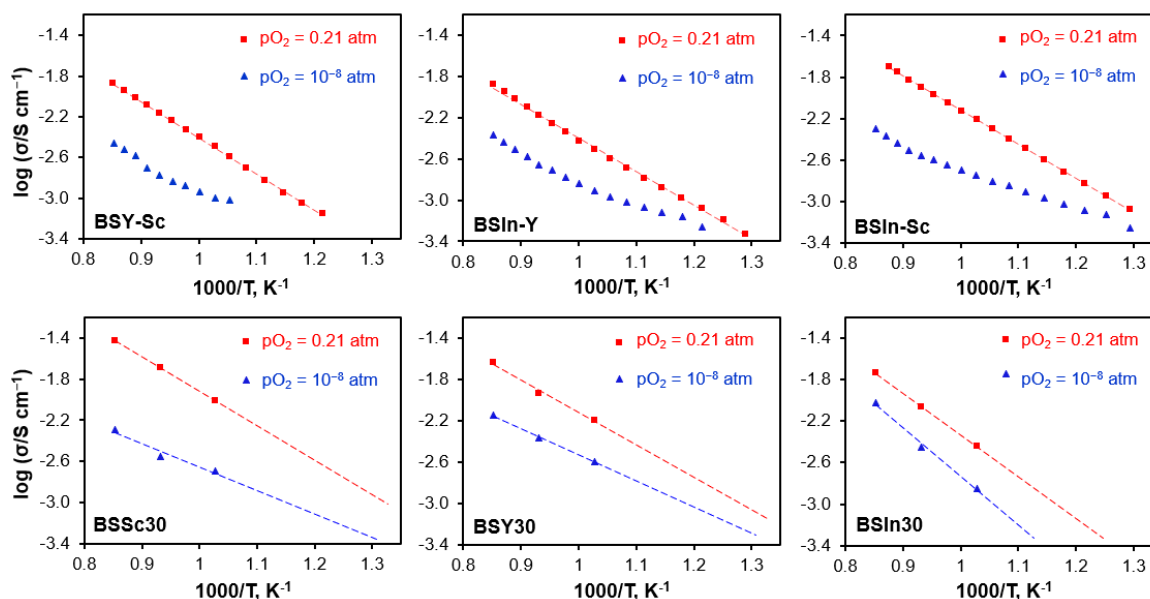

Figure 5 Total electrical conductivity measured in air ($pO_2 = 0.21$ atm) and in the ionic plateau region ($pO_2 = 10^{-8}$ atm) for ceramic samples: co-doped $BaSn_{0.7}Y_{0.15}Sc_{0.15}O_{3-\delta}$ (BSY-Sc), $BaSn_{0.7}In_{0.15}Y_{0.15}O_{3-\delta}$ (BSIn-Y) and $BaSn_{0.7}In_{0.15}Sc_{0.15}O_{3-\delta}$ (BSIn-Sc) vs. single-doped $BaSn_{0.7}(Sc/Y/In)_{0.3}O_{3-\delta}$ [19,25].
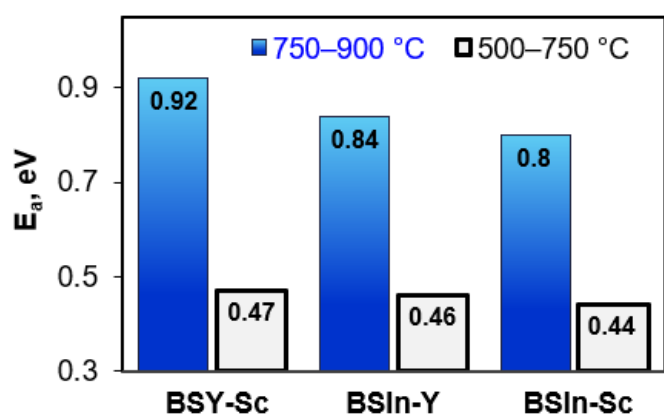
Figure 6 Apparent activation energies (E_a) for the co-doped BaSn$_{0.7}$Y$_{0.15}$Sc$_{0.15}$O$_{3-\delta}$ (BSY-Sc), BaSn$_{0.7}$In$_{0.15}$Y$_{0.15}$O$_{3-\delta}$ (BSIn-Y) and BaSn$_{0.7}$In$_{0.15}$Sc$_{0.15}$O$_{3-\delta}$ (BSIn-Sc) samples in high-temperature (750–900 °C) and intermediate-temperature (500–750 °C) ranges at pO$_2$ = 10^{-8} atm.

The values of apparent activation energy (E_a) can be used to confirm conclusions regarding the nature of charge carriers in the complex oxides [36]. The E_a values for the co-doped samples in the regions of high (750–900 °C) and medium (500–750 °C) temperatures at pO$_2$ = 10^{-8} atm are presented in Figure 6. The E_a values reach of 0.45 ± 0.02 eV at 500–750 °C, indicating the predominance of proton transport characterized by 0.5 eV or less. In the high temperature region, the E_a values reach 0.86 ± 0.06 eV. These findings indicate that oxygen ions contribute significantly to the total conductivity, considering their thermally activated conductivity behavior.

Figure 7 summarizes the electrical conductivity data for both co-doped and single-doped barium stannates. In the electrolytic region (pO$_2$ = 10^{-8} atm), the ionic conductivity of the yttrium co-doped materials is lower compared to the single-doped ones, Figure 7a. Conversely, the ionic conductivity of BSIn-Sc co-doped barium stannate demonstrates a close value with single-doped BaSn$_{0.7}$Sc$_{0.3}$O$_{3-\delta}$ (BSSc) reaching ~ 2 mS·cm^{-1} at 700 °C.

The total electrical conductivity of the samples measured in air (Figure 7b) represents the resulting contribution of both ionic and hole conductivities:

$$\sigma_{total} = \sigma_{ion} + \sigma_p, \qquad (3)$$

where, σ_{ion} and σ_p represent the ionic and p-type electronic partial conductivities, respectively. Since the value of the n-type electronic conductivity under oxidizing conditions is negligible, the hole conductivity was calculated as a difference between the total conductivity and the ionic one, as shown in Figure 7c.

Similar calculations were performed for the literature data on the conductivity of single-doped barium stannates.

The hole conductivity in proton-conducting oxides is assumed to be a factor, which reduces energy conversion efficiency of electrochemical devices due to electronic leakage and internal short-circuit effects [37, 38]. In this aspect, materials with a minimized hole component contribution are more favorable as proton-conducting electrolytes for protonic ceramic fuel cells (PCFCs) and protonic ceramic electrolysis cells (PCECs). A decrease in hole conductivity was found for the BSIn-Y and BSY-Sc samples compared to the single-doped counterparts. However, this advantage is mitigated by a corresponding decrease in ionic conductivity.
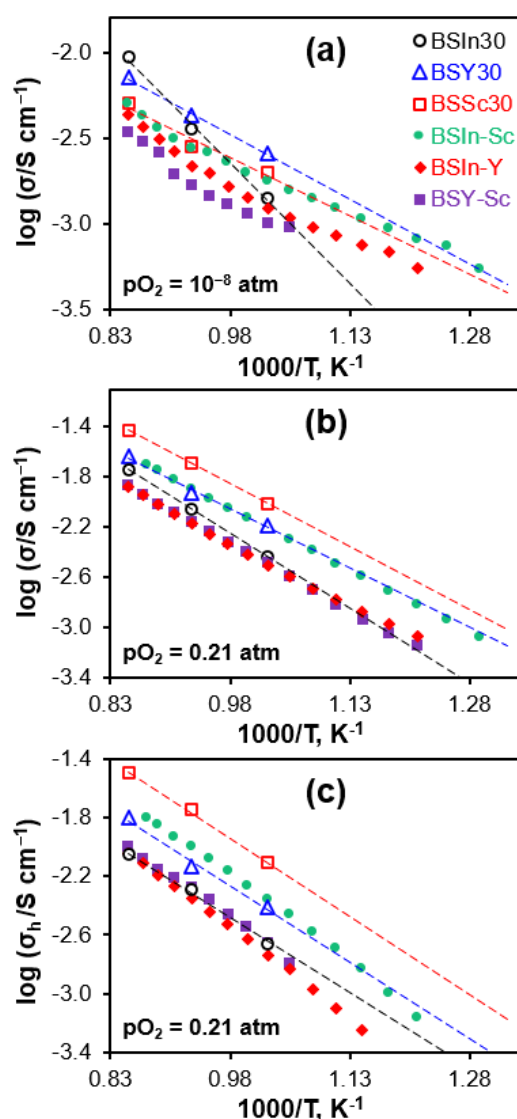

Figure 7 Summarized electrical conductivity data for both co-doped and single-doped barium stannates: **(a)** the total conductivity at pO$_2$ = 0.21 atm; **(b)** the total conductivity at pO$_2$ = 10^{-8} atm; **(c)** the calculated hole conductivity at pO$_2$ = 0.21 atm.
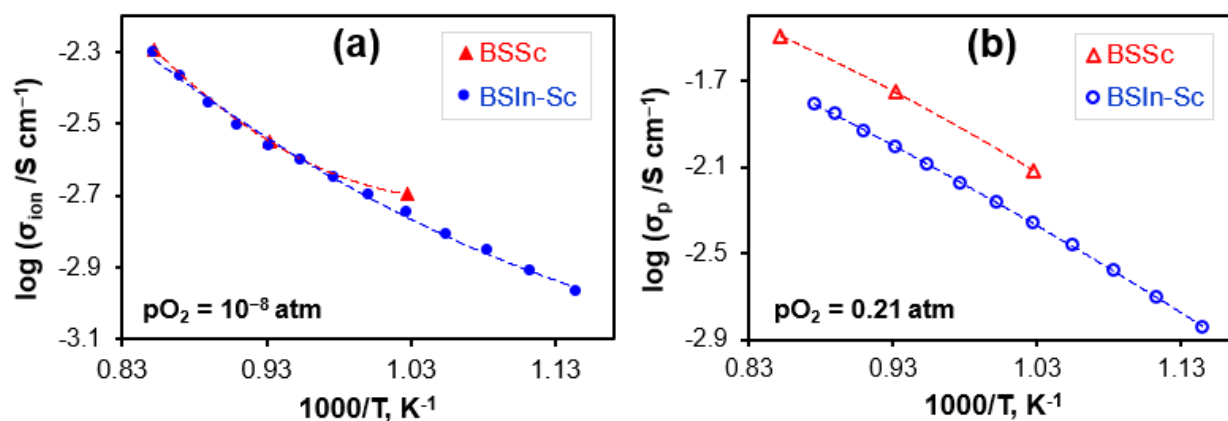
Figure 8 Temperature dependences of electrical conductivity of $BaSn_{0.7}In_{0.15}Sc_{0.15}O_{3-\delta}$ (BSIn-Sc) vs. $BaSn_{0.7}Sc_{0.3}O_{3-\delta}$ (BSSc) [19] ceramic samples: (a) ionic conductivity, (b) hole conductivity.

More interesting dependences were obtained for the BSSc, BSIn, BSIn-Sc ceramic materials. The highest and lowest hole conductivity values were found for BSSc (7.7 mS·cm⁻¹ at 700 °C) and BSIn (2.2 mS·cm⁻¹ at 700 °C), respectively. The co-doped BSIn-Sc demonstrated an intermediate hole conductivity value of 4.3 mS·cm⁻¹ at 700 °C. Thus, partial substitution of scandium by indium in BSSc in an equal ratio reduces the hole conductivity by about 2 times, while the level of ionic conductivity remains unchanged, as presented in detail in the Figure 8.

Table 2 provides the values of both ionic and hole conductivities at 700 °C for the state-of-the-art proton-conducting electrolyte materials. Among the listed complex oxides, the highest ionic conductivity is achieved for acceptor-doped barium cerates (up to 25 mS·cm⁻¹). In addition, barium cerates are also characterized by a low contribution of hole conductivity in air. The calculated ion transfer numbers (t_{ion}) are higher than 0.6. Despite the promising conductivity results, barium cerates are unstable in CO_2- and H_2O-containing atmospheres, limiting their application in electrochemical devices [51, 52]. It is interesting to note that the high t_{ion} values were also found for $SrZrO_3$, $CaZrO_3$ and La-based perovskites, although their ionic conductivity is by an order of magnitude lower than that of barium cerates. Doped barium stannates exhibit similar values of ionic conductivity and hole contribution to those of barium zirconates, placing them in an intermediate position among the extensively studied proton-conducting materials.

4. Conclusions

In the present work, the transport properties of proton-conducting materials based on barium stannate co-doped with combinations of In^{3+}/Y^{3+}, In^{3+}/Sc^{3+}, and Y^{3+}/Sc^{3+} cations were investigated. Ceramic samples with a cubic perovskite structure were obtained at 1450 °C for 5 h. The samples exhibited a dense microstructure with the absence of impurity inclusions and visible pores. Energy-dispersive X-ray spectroscopy analysis confirmed that the cationic composition of the sintered ceramics matches the nominal one. The electrical conductivity of the samples was thoroughly studied in terms of ionic and hole conductivity by four-probe measurement method. Co-doping with Y^{3+} cations reduces both ionic and hole conductivity compared to single-doped BSIn and BSS materials. It is found that the strategy of co-doping with In^{3+}/Sc^{3+} cations is effective for minimizing the hole conductivity contribution compared to scandium-doped barium stannates with the same acceptor dopant concentration. Nevertheless, conductivity studies in reducing atmospheres should be carried out before practical application of BSIn-Sc ceramic materials as electrolytes for SOFCs.

Supplementary materials

No supplementary materials are available.

Funding

Acknowledgments

Table 2 – Ionic and electronic conductivity values in air for various proton-conducting oxide materials at 700 °C.

Compositions		σ_{Ion} (mS · cm^{-1})	σ_{hole} (mS · cm^{-1})	t_{Ion}	Ref.
compound/system	x value				
$BaCe_{0.9}Y_{0.1}O_{3-\delta}$		25.15	16.58	0.60	[39]
$BaCe_{0.9}Nd_{0.1}O_{3-\delta}$		18.59	4.21	0.82	[40]
$BaCe_{0.65}Zr_{0.2}Y_{0.15}O_{3-\delta}$		9.77	5.47	0.64	[41]
$BaCe_{0.8-x}Sn_xYb_{0.2}O_{3-\delta}$	0.3	4.44	1.25	0.78	[42]
	0.4	1.93	0.79	0.71	[42]
	0.5	1.68	0.99	0.63	[42]
$BaZr_{0.8-x}Sn_xSc_{0.2}O_{3-\delta}$	0	5.05	11.54	0.30	[27]
	0.1	6.20	9.24	0.40	[27]
	0.2	2.85	7.64	0.27	[27]
$BaZr_{0.8}Y_{0.2-x}Sm_xO_{3-\delta}$	0	1.07	1.94	0.36	[43]
	0.05	1.01	1.83	0.36	[43]
	0.1	0.88	1.41	0.38	[43]
	0.2	0.55	1.19	0.32	[43]
$BaZr_{0.8}Gd_{0.2-x}Sc_xO_{3-\delta}$	0	0.31	1.16	0.21	[44]
	0.1	0.47	2.19	0.18	[44]
	0.2	1.16	2.88	0.29	[44]
	0.3	2.57	10.72	0.19	[44]
$BaSn_{1-x}Y_xO_{3-\delta}$	0.05	0.28	0.28	0.49	[25]
	0.1	1.05	2.55	0.29	[25]
	0.2	1.55	3.44	0.31	[25]
	0.3	2.57	6.40	0.29	[25]
	0.4	3.47	7.18	0.33	[25]
$BaSn_{0.7}Sc_{0.3}O_{3-\delta}$		2.01	7.66	0.21	[19]
$BaSn_{0.7}Y_{0.15}Sc_{0.15}O_{3-\delta}$		1.01	2.22	0.31	this work
$BaSn_{0.7}In_{0.15}Sc_{0.15}O_{3-\delta}$		1.79	4.34	0.29	this work
$BaSn_{0.7}In_{0.15}Y_{0.15}O_{3-\delta}$		1.24	1.84	0.40	this work
$BaSn_{0.875}Y_{0.125}O_{3-\delta}$		0.37	1.02	0.27	[9]
$La_{1-x}Sr_xScO_{3-\delta}$	0.05	1.94	4.57	0.30	[45]
	0.1	8.48	17.48	0.33	[45]
$La_{1-x}Sr_xYbO_{3-\delta}$	0.05	1.39	1.30	0.52	[46]
	0.1	3.05	3.09	0.50	[46]
$La_{1-x}Ba_xYbO_{3-\delta}$	0.05	2.40	1.68	0.59	[46]
	0.1	1.79	1.19	0.60	[46]
$La_{1-x}Ca_xYbO_{3-\delta}$	0.05	0.53	0.33	0.62	[46]
	0.1	0.68	0.23	0.74	[46]
$La_{1-x}Ca_xScO_{3-\delta}$	0.03	0.43	0.53	0.45	[47]
	0.05	3.75	7.98	0.32	[47]
	0.1	3.29	5.68	0.37	[47]
$CaZr_{0.9}Sc_{0.1}O_{3-\delta}$		0.41	0.28	0.60	[48]
$CaZr_{0.95}Sc_{0.05}O_{3-\delta}$		1.17	0.04	0.97	[49]
$CaZr_{0.9}In_{0.1}O_{3-\delta}$		0.11	0.05	0.69	[49]
$Sr_{0.98}Zr_{0.95}Yb_{0.05}O_{3-\delta}$		1.42	0.76	0.65	[50]

Author contributions

George Starostin: Investigation; Visualization; Software; Resources; Validation.

Mariam Akopyan: Resources; Investigation; Formal analysis.

Inna Starostina: Conceptualization; Software; Data curation; Supervision; Writing – Original draft.

Dmitry Medvedev: Methodology; Project administration; Writing – Original draft; Writing – Review & Editing.

Conflict of interest

The authors declare no conflict of interest.

Additional information

G.N. Starostin: AuthorId=57882347600.
M.T. Akopyan: AuthorId=57891719000.
I.A. Starostina: AuthorId=58655593700.
D.A. Medvedev: AuthorId=56007318500.

IHTE site: https://ihte.ru/?page_id=3106.
Lab sites: https://ihte.ru/?page_id=3787 (IHTE),
https://www.researchgate.net/lab/Lab-of-electrochemical-devices-based-on-solid-oxide-proton-electrolytes-Dmitry-Medvedev (ResearchGate),
https://colab.ws/labs/610 (CoLab).

References

1. Filippov SP, Yaroslavtsev AB, Hydrogen energy: development prospects and materials, Russ. Chem. Rev., **90(6)** (2021) 627–643. https://doi.org/10.1070/RCR5014

2. Ishaq H, Dincer I, Crawford C, A review on hydrogen production and utilization: challenges and opportunities, Int. J. Hydrogen Energy, **47(62)** (2022) 26238–26264. https://doi.org/10.1016/j.ijhydene.2021.11.149

3. Hauch A, Küngas R, Blennow P, Hansen AB, et al., Recent advances in solid oxide cell technology for electrolysis, Science, **370(6513)** (2020) eaba6118. https://doi.org/10.1126/science.aba6118

4. Gómez SY, Hotza D, Current developments in reversible solid oxide fuel cells, Renew. Sustain. Energy Rev., **61** (2016) 155–174. https://doi.org/10.1016/j.rser.2016.03.005

5. da Silva FS, de Souza TM, Novel materials for solid oxide fuel cell technologies: A literature review, Int. J. Hydrogen Energy, **42(41)** (2017) 26020–26036. https://doi.org/10.1016/j.ijhydene.2017.08.105

6. Zhang J, Ricote S, Hendriksen PV, Chen Y, Advanced materials for thin-film solid oxide fuel cells: recent progress and challenges in boosting the device performance at low temperatures, Adv. Funct. Mater., **32(22)** (2022) 2111205. https://doi.org/10.1002/adfm.202111205

7. Hossain S, Abdalla AM, Jamain SNB, Zaini JH, et al., A review on proton conducting electrolytes for clean energy and intermediate temperature-solid oxide fuel cells, Renew. Sustain. Energy Rev., **79** (2017) 750–764. https://doi.org/10.1016/j.rser.2017.05.147

8. Zhang W, Hu YH, Progress in proton-conducting oxides as electrolytes for low-temperature solid oxide fuel cells: from materials to devices, Energy Sci. & Eng., **9(7)** (2021) 984–1011. https://doi.org/10.1002/ese3.886

9. Wang Y, Chesnaud A, Bevillon E, Dezanneau G, Properties of Y-doped BaSnO₃ proton conductors, Solid State Ion., **214** (2012) 45–55. https://doi.org/10.1016/j.ssi.2012.02.045

10. Kim J, Sengodan S, Kim S, Kwon O, et al., Proton conducting oxides: A review of materials and applications for renewable energy conversion and storage, Renew. Sustain. Energy Rev., **109** (2019) 606–618. https://doi.org/10.1016/j.rser.2019.04.042

11. Kreuer KD, Proton-conducting oxides, Annu. Rev. Mater. Res., **33(1)** (2003) 333–359. https://doi.org/10.1146/annurev.matsci.33.022802.091825

12. Wang S, Shen J, Zhu Z, Wang Z, et al., Further optimization of barium cerate properties via co-doping strategy for potential application as proton-conducting solid oxide fuel cell electrolyte, J. Power Sources, **387** (2018) 24–32. https://doi.org/10.1016/j.jpowsour.2018.03.054

13. Fabbri E, Markus I, Bi L, Pergolesi D, et al., Tailoring mixed proton-electronic conductivity of BaZrO3 by Y and pr co-doping for cathode application in protonic SOFCs, Solid State Ion., **202(1)** (2011) 30–35. https://doi.org/10.1016/j.ssi.2011.08.019

14. Wang Y, Chesnaud A, Bevillon E, Huang J, et al., Preparation and characterization of In-substituted BaSnO₃ compounds, Funct. Mater. Lett., **06(04)** (2013) 1350041. http://dx.doi.org/10.1142/S1793604713500410

15. Ito T, Nagasaki T, Iwasaki K, Yoshino M, et al., Location of deuterium atoms in BaSn₀.₅In₀.₅O₂.₇₅₊δ at 77–473 K by neutron powder diffraction, Solid State Ion., **178(7-10)** (2007) 607–613. https://doi.org/10.1016/j.ssi.2007.01.024

16. Igawa N, Kodama K, Taguchi T, Yoshida Y, et al., Local disorder in proton conductor BaSn₀.₅In₀.₅O₂.₇₅ analyzed by neutron diffraction/atomic pair distribution function, Trans. Mater. Res. Soc. Jpn., **43(6)** (2018) 329–332. https://doi.org/10.14723/tmrsj.43.329

17. Nakamura M, Watanabe H, Akamatsu H, Fujii K, et al., Sn-based Perovskite with a wide Visible-light Absorption band Assisted by hydride Doping, Chem. Mater., **33(10)** (2021) 3631–3638. https://doi.org/10.1021/acs.chemmater.1c00460

18. Nakamura M, Akamatsu H, Fujii K, Nambu Y, et al., Synthesis of Hydride-doped Perovskite stannate with visible Light absorption Capability, Inorg. Chem., **61(17)** (2022) 6584–6593. https://doi.org/10.1021/acs.inorgchem.2c00398

19. Zvonareva IA, Mineev AM, Tarasova NA, Fu XZ, et al., High-temperature transport properties of BaSn₁₋ₓScₓO₃₋δ ceramic materials as promising electrolytes for protonic ceramic fuel cells, J. Adv. Ceram., **11(7)** (2022) 1131–1143. https://doi.org/10.1007/s40145-022-0599-x

20. Kinyanjui FG, Norberg ST, Knee CS, Ahmed I, et al., Crystal structure and proton conductivity of BaSn₀.₆Sc₀.₄O₃₋δ: insights from neutron powder diffraction and solid-state NMR spectroscopy, J. Mater. Chem. A, **4(14)** (2016) 5088–5101. https://doi.org/10.1039/C5TA09744D

21. Wang Y, Su T, Liu W, Dong Y, et al., Effect of zn contents on the microstructure and electrical properties of BaSn₀.₅Y₀.₅₋ₓZnₓO₂.₇₅ (x=0–0.04), Ceram. Int., **41(1)** (2015) 481–486. https://doi.org/10.1016/j.ceramint.2014.08.095

22. Wang Y, Su T, Liu W, Chang Q, et al., Effect of indium content on the properties of BaSn₀.₅Y₀.₅₋ₓInₓO₂.₇₅ proton conductor, Ceram. Int., **41(5)** (2015) 6863–6868. https://doi.org/10.1016/j.ceramint.2015.01.136

23. Lu N, Zhang Z, Wang Y, Li HB, et al., Enhanced low-temperature proton conductivity in hydrogen-intercalated brownmillerite oxide, Nat. Energy, **7(12)** (2022) 1208–1216. https://doi.org/10.1038/s41560-022-01166-8

24. Kochetova N, Animitsa I, Medvedev D, Demin A, et al., Recent activity in the development of proton-conducting oxides for high-temperature applications, RSC Adv., **6(77)** (2016) 73222–73268. https://doi.org/10.1039/C6RA13347A

25. Zvonareva IA, Starostin GN, Akopian MT, Vdovin GK et al., Ionic and electronic transport of dense Y-doped barium stannate ceramics for high-temperature applications, J. Power

Sources, **565** (2023) 232883. https://doi.org/10.1016/j.jpowsour.2023.232883

26. Yang JH, Kim DH, Kim BK, Kim YC, High activation energy for proton migration at Σ3111/11‾0 tilt grain boundary in barium zirconate, Solid State Ion., **252** (2013) 126–131. https://doi.org/10.1016/j.ssi.2013.07.006

27. Zvonareva IA, Kasyanova AV, Tarutin AP, Vdovin GK, et al., Enhanced transport properties of Sn-substituted proton-conducting $BaZr_{0.8}Sc_{0.2}O_{3-\delta}$ ceramic materials, J. Am. Ceram. Soc., **105(3)** (2022) 2105–2115. https://doi.org/10.1111/jace.18224

28. Klinkova LA, Nikolaichik VI, Barkovskii NV, Fedotov VK, On the existence of a homologous series of $Ba_mCu_{m+n}O_y$ oxides with the cubic structure of the $BaCuO_2$ oxide, Phys. C Supercond., **470(22)** (2010) 2067–2071. https://doi.org/10.1016/j.physc.2010.09.013

29. Yang CF, Lo SH, Grain growth for CuO-BaO mixtures added $BaTi_{1+x}O_{3+2x}$ ceramics, Mater. Res. Bull., **32(12)** (1997) 1713–1722. https://doi.org/10.1016/S0025-5408(97)00156-6

30. Amsif M, Marrero-Lopez D, Ruiz-Morales JC, Savvin SN et al., Influence of rare-earth doping on the microstructure and conductivity of $BaCe_{0.9}Ln_{0.1}O_{3-\delta}$ proton conductors, J. Power Sources, **196(7)** (2011) 3461–3469. https://doi.org/10.1016/j.jpowsour.2010.11.120

31. Gilardi E, Fabbri E, Bi L, Rupp JLM, et al., Effect of dopant–host ionic radii mismatch on acceptor-doped barium zirconate microstructure and proton conductivity, J. Phys. Chem. C, **121(18)** (2017) 9739–9747. https://doi.org/10.1021/acs.jpcc.7b02163

32. Lv J, Wang L, Lei D, Guo H, et al., Sintering, chemical stability and electrical conductivity of the perovskite proton conductors $BaCe_{0.45}Zr_{0.45}M_{0.1}O_{3-\delta}$ (M=In, Y, Gd, Sm), J. Alloys Compd., **467(1-2)** (2009) 376–382. https://doi.org/10.1016/j.jallcom.2007.12.103

33. Zvonareva IA, Medvedev DA, Proton-conducting barium stannate for high-temperature purposes: A brief review, J. Eur. Ceram. Soc., **43(2)** (2023) 198–207. https://doi.org/10.1016/j.jeurceramsoc.2022.10.049

34. Fabbri E, Pergolesi D, Traversa E, Materials challenges toward proton-conducting oxide fuel cells: a critical review, Chem. Soc. Rev., **39(11)** (2010) 4355. https://doi.org/10.1039/B902343G

35. Han D, Toyoura K, Uda T, Protonated $BaZr_{0.8}Y_{0.2}O_{3-\delta}$: impact of hydration on electrochemical Conductivity and local Crystal Structure, ACS Appl. Energy Mater., **4(2)** (2021) 1666–1676. https://doi.org/10.1021/acsaem.0c02832

36. Sun W, Liu M, Liu W, Chemically stable yttrium and tin co-doped barium zirconate electrolyte for next generation high performance proton-conducting solid oxide fuel cells, Adv. Energy Mater., **3(8)** (2013) 1041–1050. https://doi.org/10.1002/aenm.201201062

37. Kasyanova AV, Zvonareva IA, Tarasova NA, Bi L, et al., Electrolyte materials for protonic ceramic electrochemical cells: main limitations and potential solutions, Mater. Rep.: Energy, **2(4)** (2022) 100158. https://doi.org/10.1016/j.matre.2022.100158

38. Qiu R, Lian W, Ou Y, Tao Z, et al., Multifactor theoretical analysis of current leakage in proton-conducting solid oxide fuel cells, J. Power Sources, **505** (2021) 230038. https://doi.org/10.1016/j.jpowsour.2021.230038

39. Oishi M, Akoshima S, Yashiro K, Sato K, et al., Defect structure analysis of B-site doped perovskite-type proton conducting oxide $BaCeO_3$, Solid State Ion., **179(39)** (2008) 2240–2247. http://dx.doi.org/10.1016/j.ssi.2008.08.005

40. Oishi M, Akoshima S, Yashiro K, Sato K, et al., Defect structure analysis of proton-oxide ion mixed conductor $BaCe_{0.9}Nd_{0.1}O_{3-\delta}$, Solid State Ion., **181(29-30)** (2010) 1336–1343. https://doi.org/http://dx.doi.org/10.1016/j.ssi.2010.07.034

41. Lim DK, Park CJ, Choi MB, Park CN, et al., Partial conductivities of mixed conducting $BaCe_{0.65}Zr_{0.2}Y_{0.15}O_{3-\delta}$, Int. J. Hydrogen Energy, **35(19)** (2010) 10624–10629. http://dx.doi.org/10.1016/j.ijhydene.2010.07.122

42. Zvonareva IA, Tarutina LR, Vdovin GK, Lyagaeva JG, et al., Heavily Sn-doped barium cerates $BaCe_{0.8-x}Sn_xYb_{0.2}O_{3-\delta}$: correlations between composition and ionic transport, Ceram. Int., **47(18)** (2021) 26391–26399. https://doi.org/10.1016/j.ceramint.2021.06.050

43. Zhu Z, Wang S, Investigation on samarium and yttrium co-doping barium zirconate proton conductors for protonic ceramic fuel cells, Ceram. Int., **45(15)** (2019) 19289–19296. https://doi.org/10.1016/j.ceramint.2019.06.179

44. Qin G, Bao J, Gao J, Ruan F, et al., Enhanced grain boundary conductivity of Gd and Sc co-doping $BaZrO_3$ proton conductor for proton ceramic fuel cell, Chem. Eng. J., **466** (2023) 143114. https://doi.org/10.1016/j.cej.2023.143114

45. Lesnichyova AS, Belyakov SA, Stroeva AY, Kuzmin AV, Proton conductivity and mobility in Sr-doped $LaScO_3$ perovskites, Ceram. Int., **47(5)** (2021) 6105–6113. https://doi.org/10.1016/j.ceramint.2020.10.189

46. Kasyanova AV, Lyagaeva JG, Vdovin GK, Murashkina AA, et al., Transport properties of $LaYbO_3$-based electrolytes doped with alkaline earth elements, Electrochimica Acta, **439** (2023) 141702. https://doi.org/10.1016/j.electacta.2022.141702

47. Lesnichyova A, Stroeva A, Belyakov S, Farlenkov A, et al., Water uptake and transport properties of $La_{1-x}Ca_xScO_{3-\alpha}$ proton-conducting oxides, Materials, **12(14)** (2019) 2219. http://dx.doi.org/10.3390/ma12142219

48. Ding Y, Li Y, Huang W, Influence of grain interior and grain boundaries on transport properties of scandium-doped calcium zirconate, J. Am. Ceram. Soc., **103(4)** (2020) 2653–2662. https://doi.org/10.1111/jace.16968

49. Lyagaeva J, Danilov N, Korona D, Farlenkov A, et al., Improved ceramic and electrical properties of $CaZrO_3$-based proton-conducting materials prepared by a new convenient combustion synthesis method, Ceram. Int., **43(9)** (2017) 7184–7192. http://dx.doi.org/10.1016/j.ceramint.2017.03.006

50. Khaliullina A, Meshcherskikh A, Dunyushkina L, Effect of cation nonstoichiometry on hydration and charge transport processes in Yb-doped $SrZrO_3$ perovskite-type proton conductor for ceramic electrochemical cells, Processes, **11(10)** (2023) 2939. https://doi.org/10.3390/pr11102939

51. Lu J, Wang L, Fan L, Li Y, et al., Chemical stability of doped $BaCeO_3$-$BaZrO_3$ solid solutions in different atmospheres, J. Rare Earths, **26(4)** (2008) 505–510. https://doi.org/10.1016/S1002-0721(08)60127-1

52. Medvedev DA, Lyagaeva JG, Gorbova EV, Demin AK, et al., Advanced materials for SOFC application: strategies for the development of highly conductive and stable solid oxide proton electrolytes, Prog. Mater. Sci., **75** (2016) 38–79. http://dx.doi.org/10.1016/j.pmatsci.2015.08.001